IEEE Photonics Journal
An IEEE Photonics Society Publication

Open Access

Super-Strong Photonic Localizations in Symmetric Defect Waveguide-Ring Networks

Volume 9, Number 2, April 2017

Xubo Hu
Xiangbo Yang
Dongmei Deng

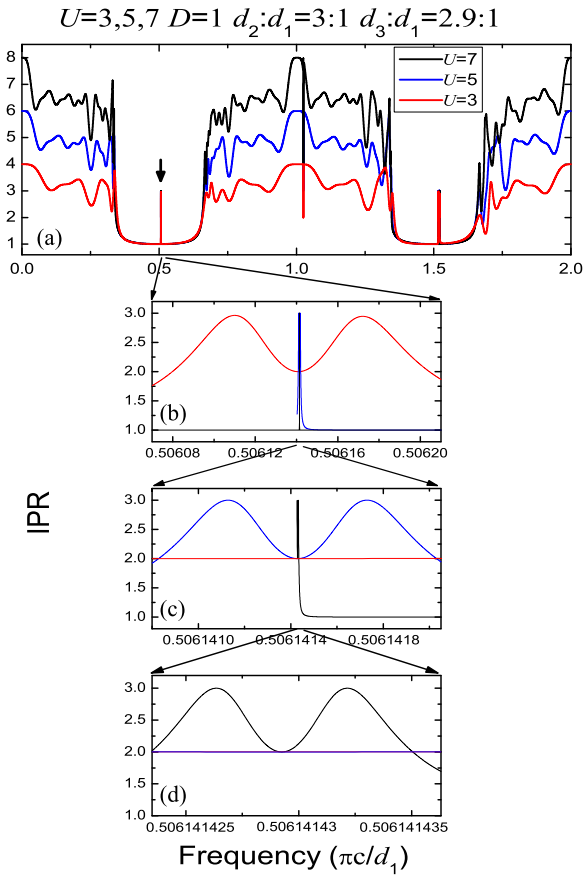

DOI: 10.1109/JPHOT.2017.2684708
1943-0655 © 2017 IEEE

IEEE photonics SOCIETY

IEEE

Super-Strong Photonic Localizations in Symmetric Defect Waveguide-Ring Networks

Xubo Hu,[1,2] **Xiangbo Yang,**[1] **and Dongmei Deng**[1]

[1]Guangdong Provincial Key Laboratory of Nanophotonic Functional Materials and Devices, South China Normal University, Guangzhou 510631, China
[2]College of Electronic Engineering, South China Agricultural University, Guangzhou 510642, China

DOI:10.1109/JPHOT.2017.2684708

Manuscript received February 17, 2017; revised March 15, 2017; accepted March 16, 2017. Date of publication March 20, 2017; date of current version April 14, 2017. This work was supported in part by the National Natural Science Foundation of China under Grant 11374107, Grant 11674107, and Grant 11374108; in part by the Natural Science Foundation of Guangdong Province under Grant 2015A030313374, and in part by the Scientific Research Foundation of Graduate School of South China Normal University under Graduate Grant 2015lkxm27. Corresponding author: Xiangbo Yang (e-mail: xbyang@scnu.edu.cn).

Abstract: Super-strong photonic localizations that occur in symmetric defect waveguide-ring networks (SDWRNs) are presented in this study. It is found that the intensity of maximal photonic localization can increase as an exponential function with the number of rings and as a power function with the breaking degree of a defect in SDWRNs. Compared with previous reported results, SDWRNs can generate stronger photonic localizations and possess simpler structures. The fitting formulas of the intensity have been obtained. Moreover, the intensity, site number, and site positions for the maximal photonic localization can be adjusted by changing structural parameters in SDWRNs. The study may provide attractive applications as multichannel high efficiency energy storages, narrow-bandwidth filters, optical switches, and other correlative optical devices.

Index Terms: Localization, symmetric defect waveguide-ring networks (SDWRNs), waveguide.

1. Introduction

Since the discovery of photonic band gaps (PBG) in photonic crystals [1], much attention has been paid to the investigation of PBG materials [2]–[11]. When electromagnetic (EM) waves propagate through PBG materials, they exhibit PBG and photonic localizations. This provides probabilities to control and manipulation the propagation of EM waves. Numerous optic devices like random lasers [12], resonators [13], narrow-bandwidth filters [14], optical switches [15], and multi-channel high efficiency energy storages [16]–[17] can be designed via light confinement from localization. Photonic localizations in quasi-periodic structures [18]–[19] and random structures [20]–[21] have been studied intensively. In photonic crystals with defect photonic localizations occur because of the local geometrical and permittivity variations [22]–[23]. Some special periodic geometries permit wave localization without the presence of any defect because of destructive wave interference [24]–[25]. The optical waveguide networks (OWNs), another kind of PBG structures, have been attracted great concern because of the structural flexibility [26]–[28]. Vasseur *et al.* investigated the defect

modes in 1-D comblike photonic waveguides and found that the behavior of the localized states is analyzed as a function of the length, of the position, and of the number of defective branches [26]. Zhang *et al.* studied the localized electromagnetic waves in three-dimensional networks of waveguides and observed Anderson localized states in the presence of defects or randomness [27]. Cheng *et al.* investigated the strong localization of photonics in symmetric Fibonacci superlattices [28]. Different from photonic localizations induced by the local effect of defect in photonic crystals, OWNs can generate stronger photonic localizations because of the resonant effect in the whole networks. In experiment, using standard coaxial cables as 1-D waveguide, Zhang *et al.* [27] and Aynaou *et al.* [29] studied the localized electromagnetic waves in 3-D networks of waveguides and quasiperiodic serial loop structures, respectively. Experiments and numerical calculations are in good agreement.

Very recently, it is found that a single-optical-waveguide ring (SOWR) can generate strong photonic localizations and the intensity of maximal photonic localization increases with the increment of loop length quantum number [30]. Although the structure of a SOWR is extremely simple, SOWRs suffer three disadvantages. First, the intensity of maximal photonic localization is not large enough, which usually reaches several orders of magnitude. Second, the growth rate of intensity of photonic localization is not fast because the relation between the intensity of maximal photonic localization and loop length quantum number is a quadratic function. Third, loop length quantum number is closely related to the machining precision of waveguide length, and a large value is difficult to be achieved in experiments because of the limitations of the microfabrication technology.

As we know, because of additional light confinement photonic localization can be generated by introducing structural defects in waveguide arrays [31], and strongly localized modes with high transmission can also be found in some symmetric structures [28], [32]. Tang *et al.* proposed symmetric two-segment-connected triangular defect waveguide network (STSCTDWN) and found that strong photonic localization can be found because of the waveguide-length defects [33], [34]. Most importantly, these systems can generate the largest intensity of photonic localization which increases as an exponential function with the increment of the number of unit cells and as an inverse-squared function with the decrement of the breaking degree of defects. Although STSCTDWNs have the above advantages, they still suffer from two disadvantages. First, the structures of them are all extraordinary complex. When every two unit cells are added because of the structural symmetry, twelve waveguide segments should be added in a STSCTDWN. The more the unit cells there exist, the more the waveguide segments are needed, which increases the difficulty of implement in experiments. Second, there are only two sites of maximal photonic localizations and the site number will not increase for different STSCTDWNs. The reason is that the largest intensity of photonic localization is located at the nodes connected with continuous defects. Herein, a symmetric defect waveguide-ring network (SDWRN) is presented to improve the properties of strong localizations. The SDWRN retains the STSCTDWN structure's advantages. Furthermore, the growth rate of intensity of photonic localization in SDWRNs is larger than that in STSCTDWNs when we change the matching ratio of arm lengths in perfect rings. Most importantly, the structure is greatly simplified compared with that of STSCTDWN. Only four waveguide segments need to be added when we add two rings in a SDWRN. The simplified structure will facilitate the implementation in experiments.

Compared with aforementioned structures, SDWRNs can generate stronger photonic localizations. In addition, there are three ways of increasing intensity of maximal photonic localization: choosing suitable matching ratio of arm lengths in perfect rings, increasing the number of perfect rings, and decreasing the breaking degree of a defect. For the first way, we divide SDWRNs into three types according to the matching ratio and find that one type will generate stronger photonic localizations than the other two types. For the second way, on the condition that the machining precision of waveguide length has not been improved we can obtain stronger photonic localizations by increasing the number of perfect rings in SDWRNs, which will reduce the difficulties in microfabrication process compared with improving the precision. For the third way, in order to change the breaking degree of a defect one can change the length of one waveguide segment in same rings by temperature compensation.

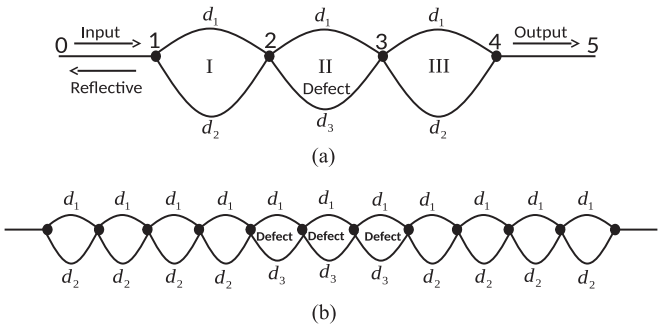

Fig. 1. Schematic diagram of the 1-D SDWRN with one entrance and one exit, where d_1 and d_2 (d_1 and d_3) are the lengths of the upper and lower arms in perfect (defect) ring, respectively. "Input," "Reflective," and "Output" represent the input, reflective, and output electromagnetic waves, respectively. (a) $U = 3$ and $D = 1$. (b) $U = 11$ and $D = 3$.

In this paper, we study the optical transmission through SDWRNs and find photonic frequency of maximal photonic localization. The relationship among the intensity of maximal photonic localization and different structural parameters are obtained. Moreover, the maximal photonic localizations exist in waveguide segments, which are larger than those at nodes. The site positions and site number of maximal photonic localizations in SDWRNs are investigated. Our results provide potential applications as multi-channel high efficiency energy storages, narrow-bandwidth filters, optical switches, and other correlative optical devices. This paper is organized as follows. In Section 2, we introduce the structure of our designed SDWRNs, generalized eigenfunction method, and the method for calculating intensity of photonic localization. The numerical results and discussions of the maximal photonic localizations in SDWRNs are presented in Section 3. Finally, a conclusion is given in Section 4.

2. Model and Methods

2.1 Model

In [34] it is found that strong photonic localization can be generated because of resonance effects induced by continuous and symmetrical waveguide-length defects. If a waveguide network contains continuous and symmetrical waveguide-length defects, strong photonic localization will be generated. We change STSCTDWNs [33], [34] into SDWRNs. This simplification can keep the property of strong localization in systems. Most importantly, the structures of SDWRNs are greatly simplified compared with STSCTDWNs, which will make the operation be more convenient in experiments.

Our studied SDWRNs are made up of 1-D vacuum optical waveguide segments and designed as follows: this kind of networks contain an odd number of rings, where an odd number of defect rings are located continuously and symmetrically in the middle of the systems while an even number of perfect rings are located on the two ends of the defect rings symmetrically. In SDWRNs the defects are all waveguide-length defects, but not material defects. In our study the waveguide-length defect means that the matching ratio of the waveguide length of the lower arm to that of the upper arm (MRWL) in a defect ring will be different from the MRWL in a perfect ring. The MRWL is $d_2 : d_1 = n : 1$ in a perfect ring, and the MRWL is $d_3 : d_1 = (n \pm \Delta d) : 1$ in a defect ring; here, n is a positive integer and Δd is the breaking degree of a defect, which is ordered as $0 < \Delta d \leq 0.1$. i.e., there is a waveguide-length flaw in a defect ring compared to a perfect ring.

As an example, we plot the SDWRN with one defect in Fig. 1(a). The SDWRN with three rings, one entrance and one exit can be seen in Fig. 1(a). Rings I and III are perfect rings and ring II is a defect ring. d_1, d_2 and d_3 are three kinds of waveguide lengths. Both the lengths of the optical waveguide segments connected with the entrance and exit are all d_1. U and D denote the numbers of all the rings and the defect rings in SDWRNs, respectively. For example, in the system shown

in Fig. 1(a), $U = 3$, $D = 1$. In order to make clear the symmetry of defects, we plot the SDWRN with $U = 11$ and $D = 3$ in Fig. 1(b). From Fig. 1(b) one can see that three defect rings are located continuously and symmetrically in the middle of the systems while eight perfect rings are located on the two ends of the defect rings symmetrically.

2.2 Generalized Eigenfunction Method

In our study the networks are formed by segments of 1-D waveguides, where only monomode propagation of EM waves needs to be considered [35]. The EM wave function with angular frequency ω in any segment between nodes i and j can be regarded as a linear combination of two opposite traveling plane waves [35]:

$$\psi_{ij}(x) = A_{ij}e^{\imath kx} + B_{ij}e^{-\imath kx} \tag{1}$$

where the wave vector $k = \omega/c$ and c is the speed of the EM wave in the vacuum. The wave function is continuous at each node:

$$\begin{cases} \psi_{ij}\big|_{x=0} = \psi_i \\ \psi_{ij}\big|_{x=l_{ij}} = \psi_j \end{cases} \tag{2}$$

where ψ_i and ψ_j are the wave functions at nodes i and j, respectively, and l_{ij} is the length of the waveguide between nodes i and j. From (1) and (2), one can get

$$\psi_{ij}(x) = \frac{\sin k\left(l_{ij} - x\right)}{\sin kl_{ij}}\psi_i + \frac{\sin kx}{\sin kl_{ij}}\psi_j. \tag{3}$$

By means of the energy flux conservation and the local coordinate system one can deduce the following network equation [35]:

$$-\psi_i \sum_j \cot kl_{ij} + \sum_j \psi_j \csc kl_{ij} = 0. \tag{4}$$

By use of (1) one can obtain the normalized wave functions of the entrance and exit as follows:

$$\begin{cases} \psi_0 = 1 + r \\ \psi_1 = e^{\imath kd_1} + re^{-\imath kd_1} \\ \psi_l = t \\ \psi_{l+1} = te^{\imath kd_1} \end{cases} \tag{5}$$

where r and t are reflection and transmission coefficients, respectively. From (4) and (5) one can obtain the relationship among the wave functions ψ_i ($i = 0, 1, 2, \cdots, l+1$) in a finite SDWRN, which is a united equation set. Solving this united equation set one can obtain the transmissivity T as follows:

$$T = |t|^2. \tag{6}$$

Evidently, it is not easy to solve the united equation set when the SDWRNs have many rings. In this paper we use the generalized eigenfunction method [35] to compute t, where the coefficients r and t are both treated as generalized wave functions. By calculating eigenvalues, one can obtain the transmissivity T and the intensity of photonic localization anywhere within a SDWRN. In this paper we define the intensity of photonic localization anywhere as

$$I(x) = \left|\psi_{ij}(x)\right|^2. \tag{7}$$

3. Numerical Results and Discussions

In this section we obtain photonic frequency of maximal photonic localization and investigate the influences of structural parameters on $I_{\max}$ in detail. It is found that the SDWRNs with

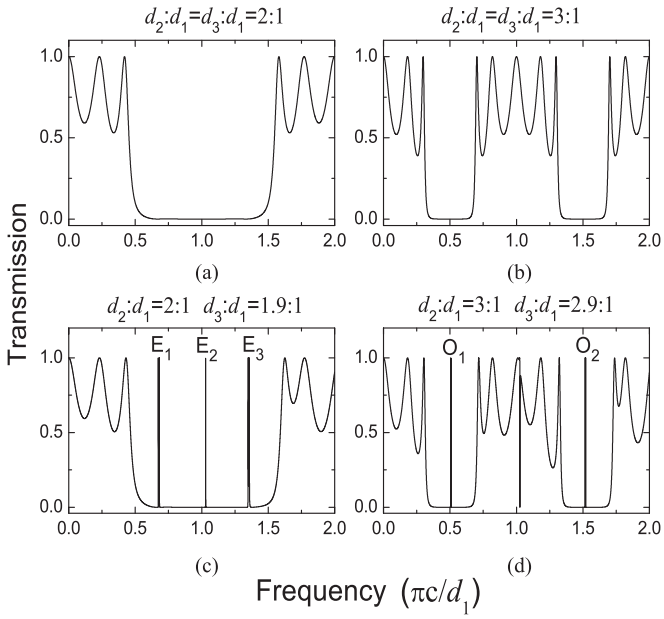

Fig. 2. Transmission spectra of the perfect systems and SDWRNs with $U = 3$, where panels (a) and (b) are the results of perfect systems and panels (c) and (d) are those of SDWRNs, where E_i ($i = 1, 2, 3$) denotes the ith group of ENFTPs of defective networks with even n, and O_i ($i = 1, 2$) denotes the ith group of ENFTPs of defective networks with odd n. The MRWLs of the four subfigures are, respectively, as follows: (a) $d_2 : d_1 = 2 : 1$, (b) $d_2 : d_1 = 3 : 1$, (c) $d_2 : d_1 = 2 : 1$ and $d_3 : d_1 = 1.9 : 1$, and (d) $d_2 : d_1 = 3 : 1$ and $d_3 : d_1 = 2.9 : 1$.

$d_3 : d_1 = (n + \Delta d) : 1$, and those with $d_3 : d_1 = (n - \Delta d) : 1$ possess identical properties of $I_{\max}$. Consequently, in this section we only investigate the latter.

3.1 Photonic Frequency of Maximal Photonic Localization

In this paper, we introduce waveguide-length defects in waveguide-ring networks. This kind of structural defects in periodic structures provides additional light confinement for localized modes to occur. By comparing the transmission spectra of defective waveguide networks with those of perfect ones, one can find that there exist several groups of extreme narrow full-transport peaks (ENFTPs) in the transmission spectra of defective waveguide networks. One ENFTP in the transmission spectra represents one localized defect mode. The defective waveguide networks naturally allow destructive waves interference, enabling localization. When the incident EM waves with the frequencies of ENFTPs propagate in our designed defective waveguide networks, strong photonic localizations occur. In this subsection, we study the rules of ENFTPs in the transmission spectra of SDWRNs in order to find the photonic frequency of maximal photonic localization. According to the numerical results we find two points as follows.

1) The group number of ENFTPs and the number of ENFTPs in each group will not change with the number of rings U and the breaking degree of a defect Δd. The number of ENFTPs can be expressed as follows. i) The group number of ENFTPs is $n + 1$ when n is even, which we label as E_i ($i = 1, 2, ..., n + 1$), respectively. For the central group $E_{\frac{n}{2}+1}$, the number of ENFTPs is equal to the number of defects D. For other group E_i ($i \neq \frac{n}{2} + 1$), the number of ENFTPs is equal to 2. ii) The group number of ENFTPs is $n - 1$ when n is odd, which we label as O_i ($i = 1, 2, ..., n - 1$), respectively. For each group O_i, the number of ENFTPs is equal to 2. In order to label each ENFTP, we mark the qth ENFTP in the mth group as O_{m-q} (E_{m-q}) for odd (even) n.

Taking SDWRNs with $U = 3$, D=1, and $n = 2, 3$ as an example, we plot the transmission spectra in Fig. 2. We also plot the transmission spectra of corresponding perfect systems for comparison.

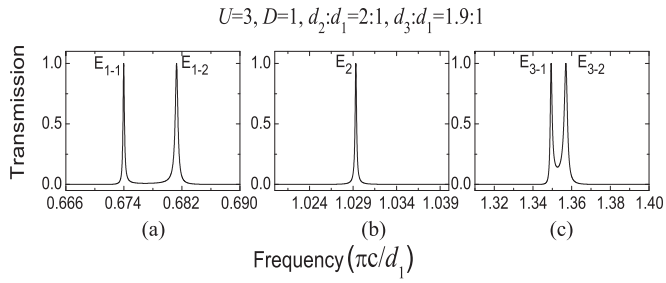

Fig. 3. Enlarged drawing of Fig. 2(c). Fine structures of (a) E_1, (b) E_2, and (c) E_3.

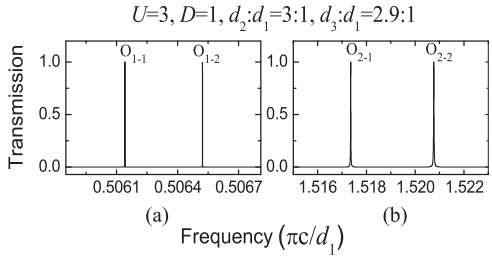

Fig. 4. Enlarged drawing of Fig. 2(d). Fine structures of (a) O_1 and (b) O_2.

From Fig. 2 one can see that there exist three (two) groups of ENFTPs in the transmission spectra for SDWRNs with $n = 2$ ($n = 3$) because of the introduction of waveguide-length defect. In order to distinguish the fine structure of each group ENFTP, we enlarge Fig. 2(c) and (d) in Figs. 3 and 4. In Fig. 3 one can see that the numbers of ENFTPs in each group are 2, 1, and 2, respectively. Accordingly, the numbers of ENFTPs in each group are both equal to 2 in Fig. 4. One can demonstrate the rule of the number of ENFTPs clearly.

2) When the frequency is in the range of 0 to $2\pi c/d_1$, the frequencies corresponding to each group of ENFTPs are about $\frac{2m}{n+1} \cdot \frac{\pi c}{d_1}$ ($m = 1, 2, ..., n$) and $\frac{\pi c}{d_1}$ when n is even; when n is odd, the frequencies corresponding to each group of ENFTPs are about $\frac{2m}{n+1} \cdot \frac{\pi c}{d_1}$ ($m = 1, 2, ..., n$) except $\frac{\pi c}{d_1}$. For example, when n is equal to 2, the frequencies corresponding to three groups of ENFTPs are about $\frac{2}{3}\frac{\pi c}{d_1}$, $\frac{\pi c}{d_1}$, and $\frac{4}{3}\frac{\pi c}{d_1}$, respectively, which can be seen in Fig. 3. When n is equal to 3, the frequencies corresponding to two groups of ENFTPs are nearly $\frac{1}{2}\frac{\pi c}{d_1}$ and $\frac{3}{2}\frac{\pi c}{d_1}$, respectively, which can be seen in Fig. 4.

The ENFTP inside the gap is due to the introduction of a defect into periodic structures and the resonance effect associated to a defect ring which plays the role of a resonator. The transmittances in the gaps are inversely proportional to gapwidth and the resonance peak is sharper corresponding to larger gapwidth [28]. According to our numerical results, only when the frequencies of the incident EM waves are those of the ENFTPs nearest to $0.5\pi c/d_1$ can the SDWRNs generate $I_{\max}$ corresponding to the sharpest resonant peak.

The SDWRNs can be divided into three types according to three types of MRWL n: even number $2m$, $4m - 1$ and $4m + 1$ types of odd number. We find that the SDWRNs with $4m - 1$ type of odd number n can generate the ENFTP nearest to the frequency $0.5\pi c/d_1$ in transmission spectra. Furthermore, it is exciting that for the SDWRNs with $4m - 1$ type of odd number n there is always one group of ENFTPs which are almost located at $0.5\pi c/d_1$ in spite of different m. On the contrary, for the SDWRNs with even number and $4m + 1$ type of odd number n, the locations of the ENFTPs near to $0.5\pi c/d_1$ change obviously for different m. Obviously, the SDWRNs with $n = 4m - 1$ can generate stronger photonic localizations than others.

In real fabrication the sizes of our designed structures can be adjusted according to the frequency of incident EM waves. For the SDWRNs with $n = 4m - 1$ which can generate stronger photonic localizations, the resonant frequency ν is about $0.5\pi c/d_1$, accordingly, $d_1 \approx \frac{0.5\pi c}{\nu}$. For example, if the frequency of incident EM waves is about 300 MHz, we can estimate the length of d_1 is about 1.57 m. In this case we can adopt the coaxial cable as the 1-D waveguide just as Zhang and Aynaou had done in [27] and [29]. For a coaxial cable, ψ denotes the voltage wave [27].

3.2 Intensity of Maximal Photonic Localization I_{max}

When the frequencies of the incident EM waves are those of the ENFTPs nearest to $0.5\pi c/d_1$, the SDWRNs can generate strongest photonic localizations. In addition, The intensity of the maximal photonic localization I_{max} is closely related to the structural parameters U, Δd, n, and D for SDWRNs. According to above discussions one knows that for the SDWRNs with $n = 4m - 1$ there is always one group of ENFTPs which are almost located at $0.5\pi c/d_1$ in transmission spectra, therefore, when the frequencies of the incident EM waves are those of the ENFTPs nearest to $0.5\pi c/d_1$, the SDWRNs with $n = 4m - 1$ can generate much larger I_{max} than those with $n \neq 4m - 1$ because of the stronger resonance effect. For comparison, we discuss the relationship among I_{max} and the structural parameters for three types of SDWRNs in this subsection.

3.2.1 Relationship Between I_{max} and Δd: From numerical results we find that the intensity of the maximal photonic localization I_{max} increases with the decrement of the breaking degree of a defect Δd. The fitting formula can be expressed as follows:

$$\log I_{max} = C_1 \log \Delta d + C_2 \tag{8}$$

where C_1 and C_2 are coefficients, and the coefficient C_1 in (8) can be shown as follows:

$$C_1 = \begin{cases} -4, & (n = 4m - 1) \\ -2, & (n = 2m) \\ -2, & (n = 4m + 1). \end{cases} \tag{9}$$

It is found that the intensity of maximal photonic localization I_{max} is inversely proportional to $(\Delta d)^4$ in SDWRNs with $n = 4m - 1$. In contrast, I_{max} is inversely proportional to $(\Delta d)^2$ in SDWRNs with $n \neq 4m - 1$. Obviously, when U and D keep constant in SDWRNs, the intensity of maximal photonic localization increases more rapidly in the SDWRNs with $n = 4m - 1$ with the decrement of Δd.

These results can be explained as follows. Due to the resonance effect induced by the waveguide-length defects, the smaller the Δd is, the sharper the resonant peak is, then the more the number of localized photonic state will be, and consequently, the larger the intensity of maximal photonic localization will be produced in SDWRNs. This is the physical mechanism that I_{max} increases with the decrement of Δd in SDWRNs. The reason is similar to that for I_{max} increases monotonously with the increment of loop length quantum number in a SOWR because it is by precisely controlling the lengths of the upper and lower arms to obtain large intensities of photonic localization in nature.

As an example, we take the SDWRNs with $n = 2, 3, 5$ as the representatives of the SDWRNs with three types of n and verify the fitting formula in (8) and (9). The numerical calculation results obtained by the method in Section 2 are labeled by dots. The line denotes the fitted curve. From Fig. 5 one can see all of dots are on the fitted curve. The numerical calculation results and the fitting results accord with each other. Additionally, with the decrement of Δd the intensity of maximal photonic localization I_{max} increases more rapidly in the SDWRNs with $n = 3$ than those in the SDWRNs with $n = 2, 5$.

3.2.2 Relationship Between I_{max} and U: The intensity of the maximal photonic localization I_{max} increases rapidly with the increment of the number of the rings U because of high reflectance when D and Δd keep constant. The relationship between I_{max} and U can be written as follows:

$$\log I_{max} = C_3 U + C_4 \tag{10}$$

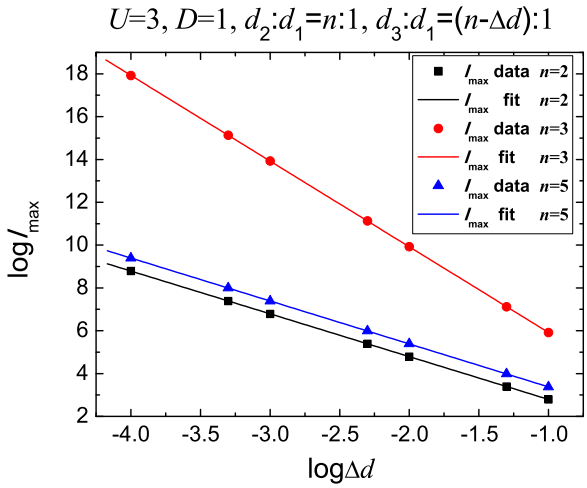

Fig. 5. $\log I_{\max}$ versus $\log \Delta d$ for the SDWRNs with $U = 3$, $D = 1$, and $n = 2, 3, 5$. The black squares, blue triangles, and red spots represent the numerical calculation results. The black line, blue line, and red line denote fitted curves.

TABLE 1
Values of Coefficients in (10) for Three Types of SDWRNs with $D = 1$ and $\Delta d = 0.1$

Type	n	C_3	C_4
$4m-1$	3	2.0187	−0.1459
	7	1.8386	0.0545
	11	1.7875	0.1260
	15	1.7731	0.1188
$4m+1$	5	0.5577	1.6929
	9	0.7690	1.3320
	13	0.8630	1.3065
	17	0.9907	1.0295
$2m$	2	0.5801	1.0491
	4	0.7770	1.3219
	6	1.0061	0.7663
	8	0.9983	1.0199

where C_3, and C_4 are coefficients. The relation between $I_{\max}$ and the number of rings U is an exponential function with constant Δd and D for SDWRNs. For the SDWRNs with $D = 1$ and $\Delta d = 0.1$ the values of coefficients C_i $(i = 3, 4)$ in (10) are shown in Table I.

In (10) $\log I_{\max}$ increases linearly with the number of rings U. From Table I one can see that the SDWRNs with $n = 4m - 1$ can generate larger $I_{\max}$ because the slope C_3 for the SDWRNs with $n = 4m - 1$ is evidently larger than those of the other two types of SDWRNs. For example, in Fig. 6 we plot the curves of $\log I_{\max}$ versus U. From Fig. 6 one can see that $\log I_{\max}$ is dependent

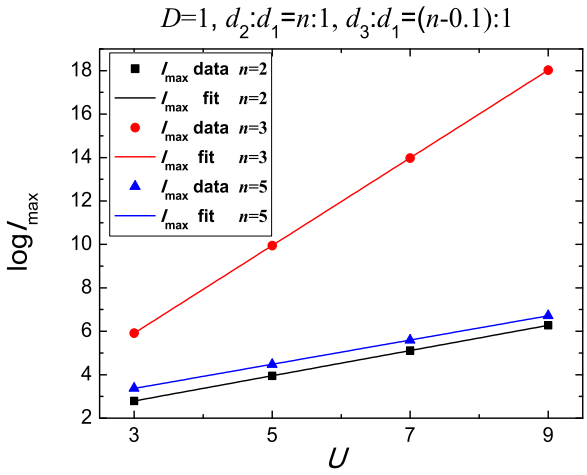

Fig. 6. I_{max} versus U for the SDWRNs with $d_2 : d_1 = n : 1$, $\Delta d = 0.1$, and $D = 1$. The black squares, blue triangles, and red spots represent the numerical calculation results. The black line, blue line, and red line denote fitted curves.

proportionally on U and this is accord with (10). Additionally, the slope for the SDWRNs with $n = 3$ is larger than those for the SDWRNs with $n = 2, 5$.

These results can be explained by the inverse participation ratio IPR. The definition of IPR can be shown as follows [27]:

$$\text{IPR} = \left(\sum_{\text{i}} |\psi|^2\right)^2 / \sum_{\text{i}} |\psi_{\text{i}}|^4. \tag{11}$$

We can use IPR as a measure of the spatial extension of a state [27]. In Fig. 7, we plot the averaged IPR as a function of frequency for three sample sizes of SDWRNs with $D = 1$, $d_2 : d_1 = 3 : 1$, $d_3 : d_1 = 2.9 : 1$, and $U = 3, 5, 7$. From Figs. 2(d), and 7(a) we can find two points as follows. (1) For frequencies in the passband, IPR approaches to the number of rings U and increases with sample size, accordingly, the states are extended ones. (2) As frequencies move into the gap, IPR is independent on the size, accordingly, the states become localized. When the frequencies are those corresponding to the ENFTPs, Fig. 7(a) can not give the fine structure of the distribution of IPR. In Fig. 7(b) we plot the enlarged drawing of the area corresponding to the first ENFTP O_{1-1}. In Fig. 7(b) there exist two peaks and one valley in the distributions of IPR for the SDWRN with $U = 3$. In order to make clear the case for the SDWRNs with $U = 5, 7$, we plot the enlarged drawings in Fig. 7(c) and (d). From Fig. 7(c) and (d) we find that the distributions of IPR for the SDWRN with $U = 5, 7$ have similar features, i.e., there exist two peaks and one valley. For some localized modes, the IPR varies with the frequency, which indicates that the mode patterns will change between on resonance and off resonance. In Fig. 7(b)–(d) the frequency corresponding to the valley is the resonance frequency of maximal photonic localization, i.e., the frequency corresponding to the ENFTP O_{1-1}. In addition, the value of IPR is always equal to 2 at the frequency of maximal photonic localization, which is a signature of localized modes. By introducing waveguide-length defect in waveguide-ring networks ENFTPs exist in the gap. At the resonance the function of the perfect rings, which are located on the two ends of the defect rings symmetrically in the SDWRN, is similar to that of the mirror in the traditional Fabry-Perot interferometers. Thus, the behavior of resonance can be analogous to the Fabry-Perot resonance. With the increment of U, the resonant peak become sharper, and the localized states with the IPR values 2 are inclined to accumulate, indicating that the density of states becomes larger. Therefore, the intensity of maximal photonic localization I_{max} increases with the increment of the number of rings U.

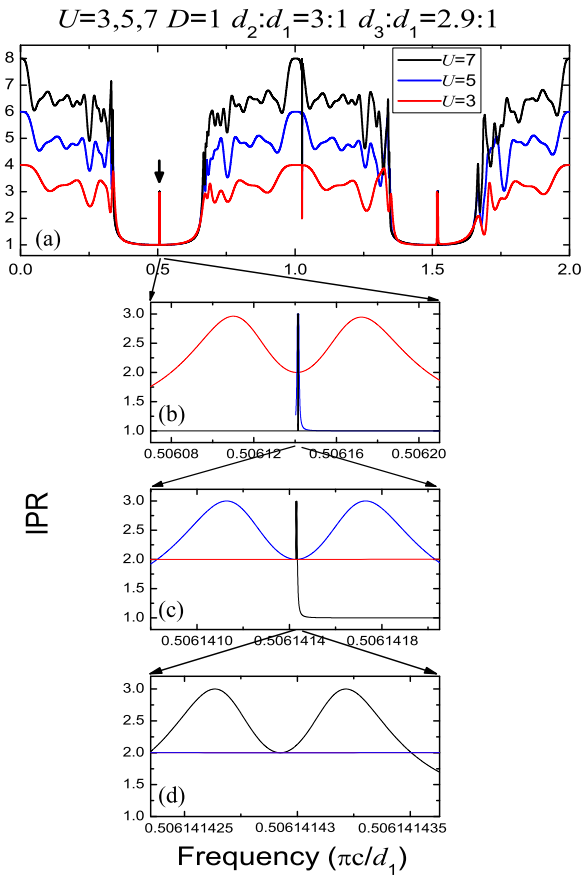

Fig. 7. Inverse participation ratio is plotted as a function of frequency for three SDWRNs with $U = 3, 5,$ and 7, respectively, where $d_2 : d_1 = 3 : 1$, $d_3 : d_1 = 2.9 : 1$, and $D = 1$. (b) Enlarged drawing of the area corresponding to the first ENFTP O_{1-1} marked by black arrow in Fig. 7(a). (c) Enlarged drawing of Fig. 7(b). (d) Enlarged drawing of Fig. 7(c).

3.2.3 Influence of D on I_{max}: According to previous discussions only the SDWRNs with $n = 4m - 1$ can generate the ENFTPs nearest to $0.5\pi c/d_1$. For unchanged Δd, $4m - 1$ and U, it is found that I_{max} decreases rapidly with the increment of D.

The reason is as follows. It is the waveguide-length defect that causes additional optical path difference and makes it possible for resonant transmission. Only when there is one defect ring in the systems the resonance effects are the most significant because of the singular variation of waveguide-length corresponding to small Δd ($0 < \Delta d \leq 0.1$). With the increment of D the influences of waveguide-length defect become weaker because defect rings increase in pairs and exhibit geometric periodicity.

As the example of $4m - 1$ type of odd number n, in Fig. 8, we use a histogram to show the relationship of $\log I_{max}$ with U and D for the SDWRNs with $d_2 : d_1 = 3 : 1$ and $d_3 : d_1 = 2.9 : 1$. In the case of U keeping unchanged $\log I_{max}$ decreases with the increment of D. On the other hand, in the case of D keeping unchanged $\log I_{max}$ increases with the increment of U.

According to above discussions, the SDWRNs with $n = 4m - 1$ and $D = 1$ can generate stronger photonic localizations than others. For example, the SDWRN with $U = 3$, $D = 1$, $d_2 : d_1 = 3 : 1$, and $d_3 : d_1 = 2.9 : 1$ is the simplest structure which can generate super-strong photonic localizations in our study. Furthermore, the intensity of maximal photonic localization I_{max} increases as an exponential function with the increment of the number of rings U and as a power function with the decrement of the breaking degree of the defect Δd, i.e., I_{max} is inversely proportional to $(\Delta d)^4$ in SDWRNs with $n = 4m - 1$. On the condition that the precision in the fabrication process could

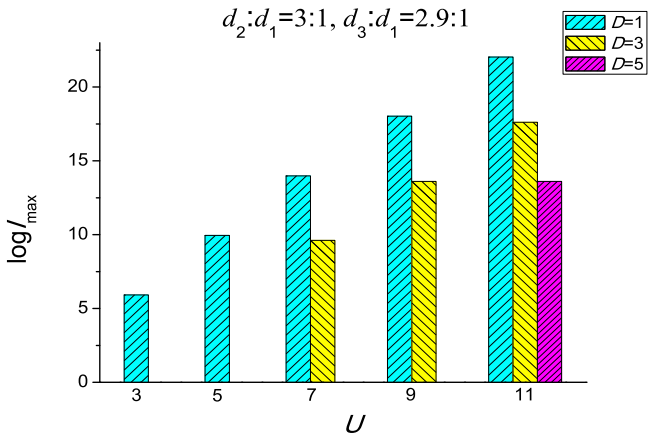

Fig. 8. logI_{max} versus U for the SDWRNs with $d_2 : d_1 = 3 : 1$ and $d_3 : d_1 = 2.9 : 1$.

not been improved, one can increase the intensity of maximal photonic localization I_{max} by three ways: choosing optimal matching ratio of arm lengths in perfect rings, i.e. $n = 4m - 1$, increasing the number of rings U in SDWRNs with $D = 1$, and decreasing the breaking degree of a defect Δd by temperature compensation. For SDWRNs increasing the number of perfect rings is easier to implement in microfabrication process compared with improving the precision. In addition, in order to change the breaking degree of a defect one can change the length of one waveguide segment in same rings by temperature compensation. In order to study the super-strong photonic localizations in SDWRNs, in the following subsection, we only discuss the SDWRNs with $n = 4m - 1$ and $D = 1$.

3.3 Site of Maximal Photonic Localizations

In this subsection, we investigate the site positions and site number of maximal photonic localizations of SDWRNs with $D = 1$ and $n = 4m - 1$. For the EM waves with the frequency of ENFTPs nearest to $0.5\pi c/d_1$, the rules of site number and site positions can be expressed as follows.

i) The site number of maximal photonic localizations is decided by n. Additionally, it will not change with U and Δd. Specifically, the site number of maximal photonic localizations is equal to $(n + 1)/2$.

ii) It is found that the sites of maximal photonic localizations are all located on the lower arm of the defect ring, i.e., they are all located on the arm which there exists a waveguide-length defect. We define the distance from the qth site of maximal photonic localization to the left node of the defect ring as x_q. x_q remains almost the same with the increment of U. In addition, x_q tends to be stable with the decrement of Δd. From numerical results, x_q can be expressed as the following equation when $\Delta d \leq 10^{-2}$:

$$x_q = 2q - 1.5, \quad q = 1, 2, ... \frac{n+1}{2}. \tag{12}$$

In order to confirm the correctness of above rules, we have studied the SDWRNs with $U = 3$, $D = 1$, $\Delta d = 0.01$, and $n = 3, 7$ as examples and obtained the distribution of the intensity of photonic localization I in Figs. 9 and 10. From Fig. 9 one can clearly see that there are two sites of maximal photonic localizations on the lower arm of the defect ring for the SDWRN with $n = 3$, and the positions of them are $x_1 = 0.5$ and $x_2 = 2.5$, respectively (shown in Fig. 9(e)). From (12) one can obtain that there are four sites of maximal photonic localizations in the SDWRN with $n = 7$, and the positions of them are $x_q = 0.5, 2.5, 4.5$, and 6.5 (q= 1, 2, 3, and 4), respectively, which are accord with the results shown in Fig. 10(e).

The determination of the site positions of the maximal photonic localization in SDWRNs helps to determine the connection positions of energy storage device. Therefore, the decided site number

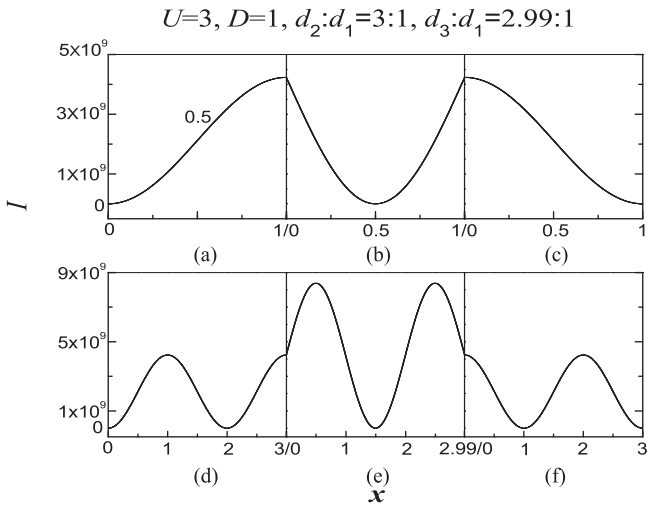

Fig. 9. Distribution of I in the SDWRNs with $U = 3$, $D = 1$, $\Delta d = 0.01$, and $n = 3$. (a) $1 - d_1 - 2$. (b) $2 - d_1 - 3$. (c) $3 - d_1 - 4$. (d) $1 - d_2 - 2$. (e) $2 - d_3 - 3$. (e) $3 - d_2 - 4$.

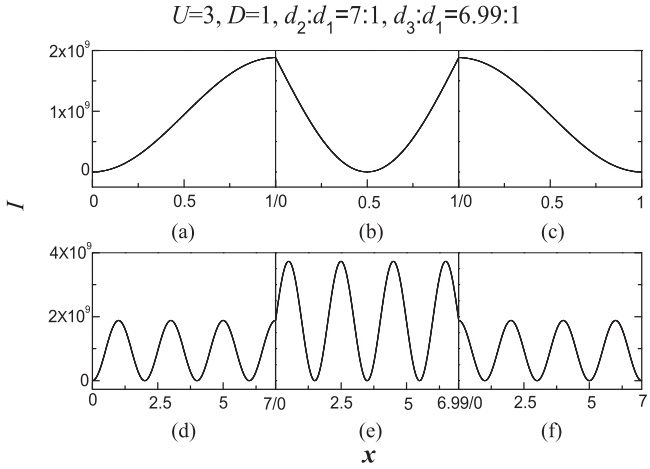

Fig. 10. Distribution of I in the SDWRNs with $U = 3$, $D = 1$, $\Delta d = 0.01$, and $n = 7$. (a) $1 - d_1 - 2$. (b) $2 - d_1 - 3$. (c) $3 - d_1 - 4$. (d) $1 - d_2 - 2$. (e) $2 - d_3 - 3$. (e) $3 - d_2 - 4$.

and site positions for constant n make SDWRNs suitable to be designed as a multi-channel high efficiency energy storage device, and it is convenient for the experimental operation.

4. Conclusion

We design SDWRNs being capable of producing super-strong photonic localizations and study the features of $I_{\max}$ and site of maximal photonic localizations.

Firstly, there exist several groups of ENFTPs in the transmission spectra of SDWRNs after introducing waveguide-length defects. We study the rules of ENFTPs and find out the photonic frequency of maximal photonic localization, i.e., only when the frequencies of the incident EM waves are those of the ENFTPs nearest to $0.5\pi c/d_1$ can the SDWRNs generate $I_{\max}$ because of the strongest resonance effect. It is found that the SDWRNs with $4m - 1$ type of odd number n can generate the ENFTP nearest to the frequency $0.5\pi c/d_1$ in transmission spectra. Furthermore, there is always one group of ENFTPs which are almost located at $0.5\pi c/d_1$ in spite of different m. Therefore, the SDWRNs with $n = 4m - 1$ can generate stronger photonic localizations than others.

Secondly, we investigate influences of structural parameters U, $\triangle d$, and D on $I_{\max}$ and obtained the fitting formulas. It is found that $I_{\max}$ increases as an exponential function with the increment of U, and $I_{\max}$ is inversely proportional to $(\triangle d)^4$ in SDWRNs with $n = 4m - 1$. In addition, $I_{\max}$ decreases rapidly with the increment of D. Obviously, the SDWRN with $U = 3$, $D = 1$, $d_2 : d_1 = 3 : 1$, and $d_3 : d_1 = 2.9 : 1$ is the simplest structure in our study. Furthermore, one can obtain stronger photonic localizations by increasing U and decreasing $\triangle d$. The former will reduce the difficulties in microfabrication process compared with improving the precision. The latter can be obtained by changing the length of one waveguide segment in same rings by temperature compensation. In addition, our studied SDWRNs can improve filtering quality as a filter. On the one hand, peaks with perfect transmission are always obtained in SDWRNs. EM waves at the full-transport resonance can tunnel through the tunneling barrier, without loss of power, but at other frequencies they are reflected. This property is important in tunable filters. On the other hand, high-Q filter structures have potential applications in optical communication applications. The Q factor of the SDWRNs can be increased by three ways: increasing the number of the rings, decreasing the breaking degree of a defect, and choosing optimal matching ratio of the waveguide length of lower to upper arm.

Finally, the site positions and site number of maximal photonic localizations are studied in SDWRNs with $D = 1$ and $n = 4m - 1$. For the EM waves with the frequency of ENFTPs nearest to $0.5\pi c/d_1$, the rules of site number and site positions can be shown as follows.(i) The site number of maximal photonic localizations is equal to $(n + 1)/2$, and it is invariable with U and $\triangle d$. (ii) The sites of maximal photonic localizations are all located on the lower arm of the defect ring. When $\triangle d \leq 10^{-2}$, x_q will satisfy the equation $x_q = 2q - 1.5, \quad q = 1, 2, ...\frac{n+1}{2}$. The decided site number and site positions for constant n make SDWRNs suitable to be designed as a multi-channel high efficiency energy storage device, and it is convenient for the experimental operation.

In conclusion, our designed SDWRNs can generate super-strong photonic localizations and possess potential applications for designing multi-channel high efficiency energy storage devices, optical switches, high power super luminescent light emitting diodes, and so on.

References

[1] E. Yablonovitch, "Inhibited spontaneous emission in solid-state physics and electronics," *Phys. Rev. Lett.*, vol. 58, no. 20, pp. 2059–2062, May 1987.

[2] S. John, "Strong localization of photons in certain disordered dielectric superlattices," *Phys. Rev. Lett.*, vol. 58, no. 23, pp. 2486–2489, Jun. 1987.

[3] S.-Y. Lin, E. Chow, V. Hietala, P. R. Villeneuve, and J. D. Joannopoulos, "Experimental demonstration of guiding and bending of electromagnetic waves in a photonic crystal," *Science*, vol. 282, no. 5387, pp. 274–276, Oct. 1998.

[4] S. Noda, K. Tomoda, N. Yamamoto, and A. Chutinan, "Full three-dimensional photonic bandgap crystals at near-infrared wavelengths," *Science*, vol. 289, no. 5479, pp. 604–606, Jul. 2000.

[5] W. Y. Zhang *et al.*, "Robust photonic band gap from tunable scatterers," *Phys. Rev. Lett.* vol. 84, no. 13, pp. 2853–2856, Mar. 2000.

[6] S. Ogawa, M. Imada, S. Yoshimoto, M. Okano, and S. Noda, "Control of light emission by 3D photonic crystals," *Science*, vol. 305, no. 5681, pp. 227–229, Jul. 2004.

[7] A. D'Orazio, M. De Sario, V. Petruzzelli, and F. Prudenzano, "Photonic band gap filter for wavelength division multiplexer," *Opt. Exp.*, vol. 11, no. 3, pp. 230–239, Feb. 2003.

[8] P. Sun and J. D. Williams, "Metallic spiral three-dimensional photonic crystal with a full band gap at optical communication wavelengths," *IEEE Photon. J.*, vol. 4, no. 4, pp. 1155–1162, Aug. 2012.

[9] M. S. Reddy, R. Vijaya, I. D. Rukhlenko, and M. Premaratne, "Low-threshold lasing in photonic-crystal heterostructures," *Opt. Exp.*, vol. 22, no. 6, pp. 6229–6238, Mar. 2014.

[10] Y.-T. Fang, H.-Q. He, and J.-X. Hu, "Transforming unidirectional edge waveguide into unidirectional air waveguide," *IEEE J. Sel. Topics Quantum Electron.*, vol. 22, no. 2, Mar./Apr. 2016, Art. no. 4901109.

[11] J.-X. Hu and Y.-T. Fang, "Self-trapped band and semi-opening movable cavity," *IEEE J. Quantum Electron.*, vol. 52, no. 7, Jul. 2016, Art. no. 6400407.

[12] Y. Yonenaga and R. Fujimura, "Random laser of dye-injected holey photonic-crystal fiber," *Phys. Rev. A*, vol. 92, no. 1, pp. 013824-1–013824-8, Jul. 2015.

[13] A. H. Safavi-Naeini, S. Gröblacher, J. T. Hill, J. Chan, M. Aspelmeyer, and O. Painter, "Squeezed light from a silicon micromechanical resonator," *Nature*, vol. 500, pp. 185–189, Aug. 2013.

[14] G. Liang, P. Han, and H. Wang, "Narrow frequency and sharp angular defect mode in 1D photonic crystals from a photonic heterostructure," *Opt. Lett.*, vol. 29, no. 2, pp. 192–194, Jan. 2004.

[15] P. Colman, P. Lunnemann, Y. Yu, and J. Mørk, "Ultrafast coherent dynamics of a photonic crystal all-optical switch," *Phys. Rev. Lett.*, vol. 117, no. 23, pp. 233901-1–233901-6, Dec. 2016.

[16] Y. Su, F. Liu, Q. Li, Z. Zhang, and M. Qiu, "System performance of slow-light buffering and storage in silicon nano-waveguide," *Proc. SPIE*, vol. 6783, Oct. 2007, Art. no. 67832.
[17] T. S. Kao, S. D. Jenkins, J. Ruostekoski, and N. I. ZheludevKao, "Coherent control of nanoscale light localization in metamaterial: creating and positioning isolated subwavelength energy hot spots," *Phys. Rev. Lett.*, vol. 106, no. 8, pp. 085501-1–085501-4, Feb. 2011.
[18] Z. V. Vardeny, A. Nahata, and A. Agrawal, "Optics of photonic quasicrystals," *Nature Photon.* vol. 7, pp. 177–187, Mar. 2013.
[19] S. M. Thon, W. T. M. Irvine, D. Kleckner, and D. Bouwmeester, "Polychromatic photonic quasicrystal cavities," *Phys. Rev. Lett.*, vol. 104, no. 24, pp. 243901-1–243901-4, Jun. 2010.
[20] J. Topolancik, B. Ilic, and F. Vollmer, "Experimental observation of strong photon localization in disordered photonic crystal waveguides," *Phys. Rev. Lett.*, vol. 99, no. 25, pp. 253901-1–253901-4, Dec. 2007.
[21] A. Z. Genack and N. Garcia, "Observation of photon localization in a three-dimensional disordered system," *Phys. Rev. Lett.*, vol. 66, no. 16, pp. 2064–2067, Apr. 1991.
[22] A. Putra, A. A. Iskandar, and M-O Tjia, "Performance enhancement of a photonic crystal microcavity and related localization of evanescent Bloch waves," *Phys. Rev. B*, vol. 84, no. 7, pp. 075159-1–075159-9, Aug. 2011.
[23] T. Baba, D. Mori, K. Inoshita, and Y. Kuroki, "Light localizations in photonic crystal line defect waveguides," *IEEE. J. Sel. Topics Quantum Electron.*, vol. 10, no. 3, pp. 484–491, May/Jun. 2004.
[24] G. Alagappan and C. E. Png, "Localization of waves in merged lattices," *Sci. Rep.*, vol. 6, Aug. 2016, Art. no. 31620.
[25] R. A. Vicencio and M. Johansson, "Discrete flat-band solitons in the kagome lattice," *Phys. Rev. A*, vol. 87, no. 6, pp. 061803-1–061803-5, Jun. 2013.
[26] J. O. Vasseur, B. Djafari-Rouhani, L. Dobrzynski, A. Akjouj, and L. Zemmouri, "Defect modes in one-dimensional comblike photonic waveguides," *Phys. Rev. B*, vol. 59, no. 20, pp. 13446–13452, May 1999.
[27] Z. Q. Zhang *et al.*, "Observation of localized electromagnetic waves in three-dimensional networks of waveguides," *Phys. Rev. Lett.*, vol. 81, no. 25, pp. 5540–5543, Dec. 1998.
[28] Y. H. Cheng, C. W. Tsao, C. H. Chen, and W. J. Hsueh, "Strong localization of photonics in symmetric Fibonacci superlattices," *J. Phys. D: Appl. Phys.*, vol. 48, no. 29, pp. 295101-1–295101-8, Jun. 2015.
[29] H. Aynaou *et al.*, "Propagation and localization of electromagnetic waves in quasiperiodic serial loop structures," *Phys. Rev. E*, vol. 72, no. 5, pp. 056601-1–056601-15, Nov. 2005.
[30] N. Wang *et al.*, "Strong photonic localization generated in single-optical-waveguide ring," *IEEE Photon. J.*, vol. 8, no. 6, Dec. 2016, Art. no. 4502513.
[31] M. I. Molina and Y. S. Kivshar, "Nonlinear localizaed modes at phase-slip defects in waveguide arrays," *Opt. Lett.*, vol. 33, no. 9, pp. 917–919, May 2008.
[32] C. W. Tsao, Y. H. Cheng, and W. J. Hsueh, "Localizaed modes in one-dimensional symmetric Thue-Morse quasicrystals," *Opt. Exp.*, vol. 22, no. 20, pp. 24378–24383, Oct. 2014.
[33] Z. Tang, X. Yang, J. Lu, and C. T. Liu, "Extreme narrow photonic passbands generated from defective two-segment-connected triangular waveguide networks," *Chin. Phys. B*, vol. 23, no. 4, pp. 044207-1–044207-8, Apr. 2014.
[34] Z. Tang, X. Yang, J. Lu, and C. T. Liu, "Super-strong photonic localization in symmetric two-segment-connected triangular defect waveguide networks," *Opt. Commun.*, vol. 331, pp. 53–58, 2014.
[35] Z.-Y. Wang and X. Yang, "Strong attenuation within the photonic band gaps of multiconnected networks," *Phys. Rev. B*, vol. 76, no. 23, pp. 235104-1–235104-7, Dec. 2007.